Diffusion Monte Carlo calculation of the phase diagram of ^{4}He on corrugated graphene

M. C. Gordillo

Departamento de Sistemas Físicos, Químicos y Naturales, Facultad de Ciencias Experimentales, Universidad Pablo de Olavide, Carretera de Utrera, km 1, 41013 Sevilla, Spain

(Received 3 December 2013; revised manuscript received 20 March 2014; published 1 April 2014)

The behavior of a ^{4}He monolayer on a single graphene sheet in which the zero-point energy of the carbon atoms was taken into account was calculated. It was found that the ground state was a liquid of density $\sim$0.030 Å^{-2}, instead of the $\sqrt{3}\times\sqrt{3}$ commensurate arrangement found previously for flat graphene. Helium absorption on both sides of the carbon layer left the phase diagram unchanged with respect to the case in which only one of the two surfaces was available for coating.

DOI: 10.1103/PhysRevB.89.155401 PACS number(s): 68.90.+g, 05.30.Jp

I. INTRODUCTION

There is an enormous amount of work devoted to the study of graphite as an adsorbent [1], both in general and in the particular case of quantum gases. Those are species light enough to manifest their bosonic or fermionic nature when the temperature is low enough. As examples of the former case, we have ^{4}He and *para*-H_2, while the latter is represented by ^{3}He. If we consider only bosonic species, it is well known that the ground state of their monolayers on graphite is either a liquid or a commensurate $\sqrt{3}\times\sqrt{3}$ solid, both structures with relatively low coverage [2–6]. When the density increases, other commensurate or incommensurate quasi-two-dimensional solids are possible, with the eventual formation of a second layer [7–10]. Those phase diagrams have been calculated using quantum Monte Carlo algorithms with good accuracy [11–18].

If we isolate any of the carbon sheets that constitute graphite, the result is graphene [19,20]. The main difference between graphene and graphite from the point of view of adsorption is that graphene has two surfaces available to be coated, in opposition to the single upper layer accessible for graphite. In addition, the carbon atoms stacked underneath that upper surface should make graphite a stronger adsorbent. This statement has not been experimentally tested, but there are some calculations supporting it [14,15,17,18]. Besides, a recent quantum calculation [21] suggests that a single graphene sheet might not behave simply as a perfectly flat graphite flake, in accordance with results of both experiments and of classical simulations [22–25]. Apparently, even at $T = 0$ K, the zero-point motion of the carbon atoms in the structure seems to be enough to make the $\sqrt{3}\times\sqrt{3}$ commensurate solid characteristic of *para*-H_2 on top of graphite much less stable than the same structure on a single flat graphene sheet. On the other hand, the energetics of the incommensurate triangular solid phase remained largely unchanged. All together this meant that the ground state of that molecular isotope on top of a realistic graphene sheet was a mixture of both the $\sqrt{3}\times\sqrt{3}$ structure and a denser incommensurate one. The familiar registered solid obtained from simulations in which graphene was considered to be perfectly flat was recovered when two graphene layers were considered instead of a single one.

Our aim in this work will be to study what happens to ^{4}He on top of a single sheet of graphene in which the zero-point motion of the carbon atoms was taken into account, affording a comparison with previous results on graphene. We considered only coverages in the monolayer range. In the next section, we will explain how we solved the Schrödinger equation for the entire system of helium atoms adsorbed on the carbon layer, the following section being devoted to describing the phase diagram derived from those calculations. Adsorption of ^{4}He on one and both graphene surfaces will be considered. We will close with some conclusions.

II. METHOD

The adsorption of quantum gases on graphite and graphene is usually studied at very low temperatures, in the limit $T \to 0$ K. This means that the ground state of a set of ^{4}He atoms on top of a carbon layer should give a reasonable description of the system. The standard technique to obtain such a ground state is the diffusion Monte Carlo (DMC) method [26], even tough finite temperature path-integral Monte Carlo calculations could be used to the task [27–29]. In DMC, the starting point is the so-called *trial* function, that contains all the information known *a priori* about the entire ensemble of atoms and molecules and can be thought of as the initial approximation to the ground-state wave function of the problem. In our case, and following closely Ref. [21], we have

$$\Phi_T(\mathbf{r}_1,\mathbf{r}_2,\ldots,\mathbf{r}_T) = \Phi_{He}(\mathbf{r}_1,\mathbf{r}_2,\ldots,\mathbf{r}_N) \times\Phi_C(\mathbf{r}_{N+1},\mathbf{r}_{N+2},\ldots,\mathbf{r}_T), \quad (1)$$

where $\mathbf{r}_1,\mathbf{r}_2,\ldots,\mathbf{r}_T$ are the positions of the N ^{4}He atoms and of the T-N carbon atoms. Φ_{He} and Φ_C can be written as

$$\Phi_{He}(\mathbf{r}_1,\mathbf{r}_2,\ldots,\mathbf{r}_N) = \prod_{i<j}\exp\left[-\frac{1}{2}\left(\frac{b_{\text{He-He}}}{r_{ij}}\right)^5\right] \times\prod_i\prod_J\exp\left[-\frac{1}{2}\left(\frac{b_{C-He}}{r_{iJ}}\right)^5\right] \times\prod_i\exp[-a(z_i-z_c)^2 - c(x_i-x_c)^2 - c(y_i-y_c)^2] \quad (2)$$

and

$$\Phi_C(\mathbf{r}_{N+1},\mathbf{r}_{N+2},\ldots,\mathbf{r}_T) = \prod_I\exp[-b(x_I-x_c)^2 - b(y_I-y_c)^2 - d(z_I-z_c)^2]. \quad (3)$$

In both equations, subscripts in capital letters designate carbon atoms, and small types are reserved to helium ones. Equation (2) is not exactly the same as the *trial* function used in Ref. [14] for ^{4}He on flat graphene. There, the product of the C-He Jastrow function by $\prod_i \exp[-a(z_i - z_c)^2]$ was substituted by the solution of a one-dimensional Schrödinger equation describing a single helium atom interacting with the carbon surface via a z-averaged potential. Here, we obtained $b_{\text{C-He}}$ and a by means of a variational Monte Carlo (VMC) calculation that included a single helium atom on top of a perfectly flat graphene surface. That last means that the contribution corresponding to the zero-point energy of the carbon atoms was not considered. Within this framework, we obtained $b_{\text{C-He}} = 2.3$ Å and $a = 3.1$ Å^{-2}. All the other helium parameters were taken from Ref. [14], while the necessary ones to define Eq. (3) came from Ref. [21]. Both in Eqs. (2) and (3) x_c, y_c, and z_c are the crystallographic positions of the carbon atoms in the graphene or the averaged positions of the helium atoms in the solids. If we wanted to model a liquid, we made $c = 0$.

Two forms of the C-He interaction potential were considered, the isotropic one of Ref. [30], and the anisotropic one of Ref. [31]. The phase diagrams calculated for those potentials on a perfectly flat graphene structure are slightly different [32], so one of our goals would be to see whether the potential chosen still matters on a corrugated surface. The helium-helium interaction was the standard Aziz potential [33]. To take into account the zero-point energy of the carbon atoms we had to consider also a C-C interaction. We chose the modified form of the Brenner potential of Ref. [34] to do so. In Ref. [21], it was found that the description of a clean graphene surface provided by that interaction was good. There, a DMC calculation using only Eq. (3) provided reasonable estimations for both the carbon bond and the energetics of the system. For instance, the standard deviation of the mean position of the carbon atoms on the graphene sheet (plane $z = 0$) was found to be ∼4.7 pm, while the length of the C-C bond was 1.412 ± 0.047 Å. Those values were reproduced in the present set of simulations, both for the clean case and when He was adsorbed on graphene. From that starting point, we calculated the phase diagrams of helium on top of a single graphene sheet, first considering that only one of the surfaces was available for adsorption, and then making both of them accessible to helium. In all cases we considered a 44.27×42.60 Å^2 supercell, including 720 carbon atoms. The time step for the helium and carbon atoms was taken to be 1/10 of the one used in a previous simulation for helium on a flat substrate [14]. This implied simulations longer at least by an order of magnitude than for planar graphene. The calculations were considered to have converged when the standard deviation of the kinetic, potential, and total energy of the helium atoms were all lower than 1 K, the only exception being the infinite dilution limit. There, simulations twice as long as for the other helium phases rendered error bars of ∼2 K for the helium binding energy (see Table I).

III. RESULTS

From Fig. 1, we can deduce the phase diagram of helium on top of graphene obtained with the isotropic C-He potential. It corresponds to the case where there is only one graphene surface available for adsorption, while the other stays clean.

TABLE I. Summary of the energies per helium atom on single coated corrugated graphene. E_1 are the results for the C-He potential of Ref. [30], while E_2 corresponds to the ones obtained with the anisotropic interaction of Ref. [31]. IC stands for the incommensurate solid. The data for that phase come from third-order polynomial fits to the data displayed in Figs. 1 and 2.

Structure	Density (Å^{-2})	E_1 (K)	E_2(K)
Infinite dilution	0	-125 ± 2	-126 ± 2
Liquid (lower limit)	0.031 ± 0.002	-125.4 ± 0.2	-127.4 ± 0.4[a]
Liquid (upper limit)	0.040 ± 0.003	-125.2 ± 0.2	-127.4 ± 0.4[a]
$\sqrt{3} \times \sqrt{3}$	0.0636	-124.5 ± 0.5	-126.5 ± 0.5
2/5	0.0763	-121.1 ± 0.4	-122.6 ± 0.5
IC	0.0763	-123.0 ± 0.3	-123.1 ± 0.3
31/75	0.0789	-123.1 ± 0.4	-124.4 ± 0.5
IC	0.0789	-122.6 ± 0.5	-122.7 ± 0.5
3/7	0.0818	-120 ± 1	-123.0 ± 0.4
IC	0.0818	-122.0 ± 0.5	-122.1 ± 0.4
IC (lower limit)	0.084 ± 0.004	-121.4 ± 0.3	-120 ± 1[b]

[a]Density 0.030 ± 0.001 Å^{-2}, derived from a third-order polynomial fit.
[b]Density 0.089 ± 0.005 Å^{-2}, derived from a Maxwell construction.

For the sake of comparison, we included also the results for a flat carbon layer taken from Ref. [14]. We considered only coverages up to ∼0.095 Å^{-2}, which means that our results cannot be compared to those previously obtained for adsorption of helium on second and successive layers [13,18,35–38]. From that figure, we can say that the ground state of helium on graphene is a liquid, instead of the $\sqrt{3} \times \sqrt{3}$

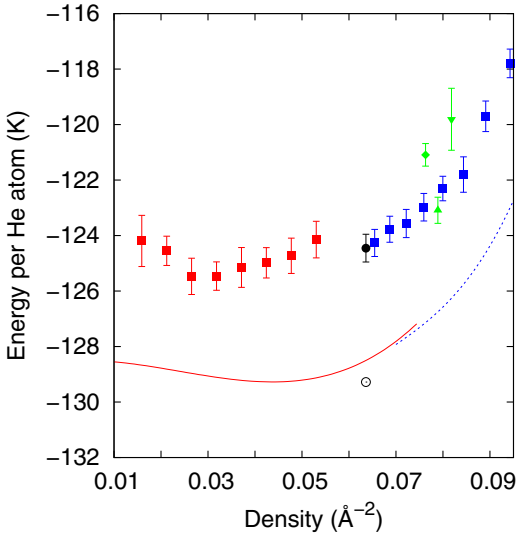

FIG. 1. (Color online) Energy per ^{4}He atom on a single graphene layer obtained using the isotropic C-He interaction. Open squares: liquid phase; full squares: incommensurate triangular phase; full circle: $\sqrt{3} \times \sqrt{3}$ commensurate structure; upward pointing triangle: 31/75 commensurate solid; downward pointing triangle: 3/7 solid; full diamond: 2/5 solid. The lines represent the results for a liquid (full) and an incommensurate (dashed) solid obtained from Ref. [14]. The open circle represents the energy per particle for a $\sqrt{3} \times \sqrt{3}$ solid also on flat graphene.

of its flat counterpart. A third-order polynomial fit (not shown) indicates that the minimum energy per helium atom corresponds to a density of 0.030 ± 0.002 Å^{-2}, lower than for flat graphene [14] ($\sim$0.044 Å^{-2}). It has also a higher energy per particle, since we go from -129.221 ± 0.009 K for the flat liquid to -125.4 ± 0.2 K for corrugated graphene.

We can see also that all phases are less stable than their corrugated counterparts. For instance, the registered 31/75 solid, stable for D_2 on graphite [6], and whose density is 0.0789 Å^{-2} (upward pointing triangle in Fig. 1), goes from an energy per particle in flat graphene of -126.50 ± 0.02 K (Ref. [14]) to -123.1 ± 0.4 K (this work). The same can be said of the 3/7 solid of density 0.0818 Å^{-2} proposed to be a stable phase for helium on graphite in Ref. [3]. It went from an energy per particle of -126.07 ± 0.01 K (Ref. [14], flat structure) to -120 ± 1 K (this work, downward pointing triangle in Fig. 1). Finally, the $\sqrt{3} \times \sqrt{3}$ commensurate arrangement of density 0.0636 Å^{-2} goes from being the ground state on flat graphene with an energy per particle of -129.282 ± 0.007 K [14] to -124.5 ± 0.5 K (full circle in Fig. 1). The other commensurate phase studied, the so-called 2/5 arrangement, follows the same trend, going from -125.81 ± 0.01 K [14] to -121.1 ± 0.4 K in this work. The remaining phase, a triangular incommensurate structure, is displayed by a set of full squares in Fig. 1, its energy per particle being also less stable than its flat counterpart.

A series of double-tangent Maxwell constructions were used to establish the sequence of stable phases when we increased the helium density. The first one is between a liquid and the single point that in Fig. 1 represents the $\sqrt{3} \times \sqrt{3}$ commensurate structure. To perform that construction, we fitted the energy per particle of the liquid to a third-order polynomial fit to the inverse of the helium density. From some points of that curve, we can draw tangent lines that end up in the single value representing the solid structure. The double-tangent Maxwell construction is the line with the minimum (in absolute value) slope, and the initial point in the curve gives us the inverse of the liquid equilibrium density. The liquid phase is then stable between the density with the minimum energy per particle to the one in equilibrium with the solid. For the isotopic potential this means the range 0.030–0.040 Å^{-2}. From the $\sqrt{3} \times \sqrt{3}$ solid up, the next stable phase is the 31/75 one, whose energy per particle is lower than that of an incommensurate arrangement of the same density (see Table I). We cannot say properly that we have made a real Maxwell construction between those commensurate solids, since both arrangements are represented by only one density, but we think we have a reasonable approximation to the real phase equilibrium. Last, a third construction between the 31/75 phase and the incommensurate one gives us a lower density limit for the latter of 0.084 ± 0.004 Å^{-2}. As we can see in Table I, neither the 2/5 or the 3/7 arrangements are stable, since their energy per particle is higher than for a triangular structure of the same density. The domain-wall structure of Refs. [11–13,18] was not contemplated here, since in graphite is an intermediate between the $\sqrt{3} \times \sqrt{3}$ and the incommensurate solids, and here we found another structure to be stable between them.

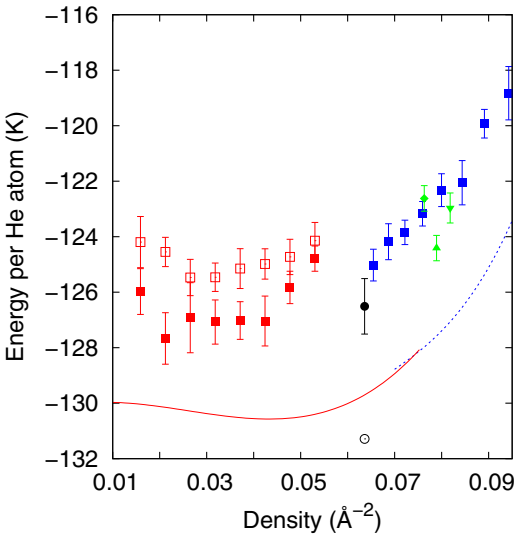

FIG. 2. (Color online) Same as in Fig. 1, but for the anisotropic C-He interaction. Open squares correspond to the liquid phase in Fig. 1 and are inserted for comparison.

Figure 2 shows a similar set of data as those of Fig. 1, but for the anisotropic C-He potential of Carlos and Cole [31]. The set of points corresponding to the liquid phase for the isotropic potential are also displayed to afford a direct comparison between Figs. 1 and 2. The use of the anisotropic interaction on a flat surface made stable with respect to the incommensurate triangular solid the $\sqrt{3} \times \sqrt{3}$, 31/75, and 3/7 phases, but not the 2/5 one [32]. They are also stable on a corrugated surface, as can be seen in Fig. 2, which is quite similar to Fig. 1. The ground state is again a liquid, of density (deduced in the same way as in the previous figure) 0.030 ± 0.001 Å^{-2} and with an energy per helium atom lower than the one from an isotropic potential. Since the tangent line of the Maxwell construction between the liquid and the $\sqrt{3} \times \sqrt{3}$ commensurate solid starts at this same density, the liquid phase is only stable at a single point, instead of the range given above for the isotropic potential. The phase changes are now liquid $\rightarrow \sqrt{3} \times \sqrt{3} \rightarrow 31/75 \rightarrow 3/7 \rightarrow$ incommensurate triangular solid with a minimum density of 0.089 ± 0.005 Å^{-2}. The energies per helium atom of all those phases are given in Table I. The only difference with the previous case is that now the 3/7 phase is stable with respect to an incommensurate one. The energies per helium atom are also lower for the anisotropic potential in all the studied commensurate arrangements. However, in the incommensurate phase, those energies are similar for both C-He interactions (see Table I for those energies at some particular densities).

Finally, Fig. 3 gives us an idea about what happens when we make both graphene surfaces available for helium coating. There, we represent the same data as in Fig. 2 as open symbols, together with their respective counterparts for double coated graphene, displayed as full symbols. The density in the x axis corresponds to the density of helium on only one surface, while the lines are third-order polynomial fits to the liquid and incommensurate triangular phase data corresponding to the situation in which both surfaces are available, intended mainly as a guide to the eye. Only stable phases were displayed

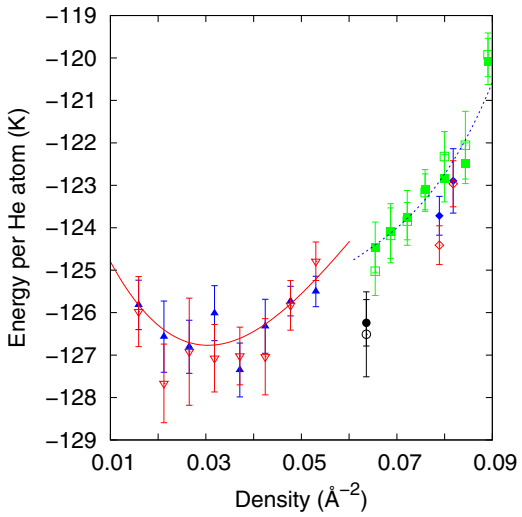

FIG. 3. (Color online) Energy per ^{4}He atom for C-He anisotropic interaction. Open symbols correspond to helium adsorbed on only one of the available graphene surfaces while full symbols represent the situation in which both surfaces are coated. Triangles: liquid phase; squares: incommensurate triangular phase; circles: $\sqrt{3} \times \sqrt{3}$ solid; diamonds: 31/75 (lower density) and 3/7 (higher density). The curves are third-order polynomial fits that serve as guides to the eye.

(not the 2/5 one). The isotropic C-He case is similar and not shown for simplicity. What we see is that, rather surprisingly, both series of data are largely compatible for the same density within their respective error bars. This is so even when the supposedly most energetic favorable situation for the solids is considered, in which the crystallographic positions share the same x_c's and y_c's coordinates for each pair of atoms located on opposite sides of the carbon layer. This is the case displayed in Fig. 3.

IV. CONCLUSIONS

The basic picture that emerges about ^{4}He adsorption of graphene from our calculations is different than the one for a perfectly flat substrate on the same substrate. In particular, the ground state seems to be a liquid irrespectively of the C-He interaction used, instead of the $\sqrt{3} \times \sqrt{3}$ times commensurate solid of Refs. [14,32]. In this, our results are similar to the experimental ones of Greywall [2,3] for graphite, in which there is an equilibrium between the liquid and the commensurate states. However, only the isotropic potential seems to produce a stable liquid in a range compatible with that deduced from calorimetric measurements ($\sim$0.04 Å^{-2}). On the other hand, a comparison to the results of Ref. [21], in which H_2 on corrugated graphene was considered, indicates that part of the discrepancy with previous calculations could be due to the fact that we considered only a single graphene sheet and not the full graphite structure. In that reference, the introduction of another graphene layer decreased further the energy per atom of the $\sqrt{3} \times \sqrt{3}$ solid. Another difference is the stabilization of the 31/75 and (for the anisotropic potential) the 3/7 phases with respect to the incommensurate solids of the same density. Even though the last solid was proposed to be stable for graphite [3], to our knowledge, there is no experimental indication of a 31/75 stable arrangement. A possible explanation could be that the energy per helium atom of the 31/75 phase for the isotropic potential is so close to the one for a triangular solid that it cannot be observed as a separate phase.

We also found that there is not much of a difference between allowing the carbon layer to be coated on one or both surfaces. Basically, this means that the energy fluctuations due to the zero-point energy of the carbon atoms are of the same order as the effect of an additional helium layer on the other side of graphene. In fact, a very recent article (Ref. [39]), in which that influence was quantified for helium clusters, found it to be at most -0.5 K per atom for big clusters, of the order of our error bars. This means that allowing the carbon atoms to move from their perfect crystallographic positions masks completely the helium-helium influence across the graphene layer.

ACKNOWLEDGMENTS

I acknowledge financial support from the Junta de Andalucía Group PAI-205, Grant No. FQM-5987, and MICINN (Spain) Grant No. FIS2010-18356.

[1] L. W. Bruch, M. W. Cole, and E. Zaremba, *Physical Adsorption: Forces and Phenomena* (Oxford University Press, Oxford, 1997).
[2] D. S. Greywall and P. A. Busch, Phys. Rev. Lett. **67**, 3535 (1991).
[3] D. S. Greywall, Phys. Rev. B **47**, 309 (1993).
[4] H. Freimuth and H. Wiechert, Surf. Sci. **162**, 432 (1985).
[5] H. Freimuth and H. Wiechert, Surf. Sci. **189-190**, 548 (1987).
[6] H. Freimuth, H. Wiechert, H. P. Schildberg, and H. J. Lauter, Phys. Rev. B **42**, 587 (1990).
[7] G. Zimmerli, G. Mistura, and M. H. W. Chan, Phys. Rev. Lett. **68**, 60 (1992).
[8] P. A. Crowell and J. D. Reppy, Phys. Rev. Lett. **70**, 3291 (1993).
[9] P. A. Crowell and J. D. Reppy, Phys. Rev. B **53**, 2701 (1996).
[10] H. Wiechert, in *Excitations in Two-Dimensional and Three-Dimensional Quantum Fluids* edited by A. G. F. Wyatt and H. J. Lauter (Plenum, New York, 1991), p. 499.
[11] M. E. Pierce and E. Manousakis, Phys. Rev. Lett. **83**, 5314 (1999).
[12] M. E. Pierce and E. Manousakis, Phys. Rev. B **62**, 5228 (2000).
[13] P. Corboz, M. Boninsegni, L. Pollet and M. Troyer, Phys. Rev. B **78**, 245414 (2008).
[14] M. C. Gordillo and J. Boronat, Phys. Rev. Lett. **102**, 085303 (2009).
[15] M. C. Gordillo and J. Boronat, Phys. Rev. B **81**, 155435 (2010).
[16] M. C. Gordillo, C. Cazorla, and J. Boronat, Phys. Rev. B **83**, 121406(R) (2011).
[17] C. Carbonell-Coronado and M. C. Gordillo, Phys. Rev. B **85**, 155427 (2012).
[18] J. Happacher, P. Corboz, M. Boninsegni, and L. Pollet, Phys. Rev. B **87**, 094514 (2013).

[19] K. S. Novoselov, A. K. Geim, S. V. Morozov, D. Jiang, Y. Zhang, S. V. Dubonos, I. V. Grigorieva, and A. A. Firsov, Science **306**, 666 (2004).
[20] K. S. Novoselov, D. Jiang, F. Schedin, T. J. Booth, V. V. Khotkevich, S. V. Morozov, and A. K. Geim, Proc. Natl. Acad. Sci. USA **102**, 10451 (2005).
[21] M. C. Gordillo, Phys. Rev. B **88**, 041406(R) (2013).
[22] J. C. Meyer, A. K. Geim, M. I. Katsnelson, K. S. Novoselov, T. J. Booth, and S. Roth, Nature (London) **446**, 60 (2007).
[23] A. Fasolino, J. H. Los, and M. I. Katnelson, Nat. Mater. **6**, 858 (2007).
[24] K. V. Zakharchenko, M. I. Katsnelson, and A. Fasolino, Phys. Rev. Lett. **102**, 046808 (2009).
[25] K. V. Zakharchenko, J. H. Los, M. I. Katsnelson, and A. Fasolino, Phys. Rev. B **81**, 235439 (2010).
[26] J. Boronat and J. Casulleras, Phys. Rev. B **49**, 8920 (1994).
[27] D. M. Ceperley, Rev. Mod. Phys. **67**, 279 (1995).
[28] M. C. Gordillo and D. M. Ceperley, Phys. Rev. B **58**, 6447 (1998).
[29] M. Boninsegni, N. Prokof'ev, and B. Svistunov, Phys. Rev. Lett. **96**, 070601 (2006).
[30] G. Stan and M. W. Cole, Surf. Sci. **395**, 280 (1998).
[31] W. E. Carlos and M. W. Cole, Surf. Sci. **91**, 339 (1980).
[32] M. C. Gordillo and J. Boronat, J. Low Temp. Phys. **171**, 606 (2013).
[33] R. A. Aziz, F. R. W. McCourt, and C. C. K. Wong, Mol. Phys. **61**, 1487 (1987).
[34] L. Lindsay and D. A. Broido, Phys. Rev. B **81**, 205441 (2010).
[35] M. E. Pierce and E. Manousakis, Phys. Rev. Lett. **81**, 156 (1998).
[36] M. E. Pierce and E. Manousakis, Phys. Rev. B **59**, 3802 (1999).
[37] M. E. Pierce and E. Manousakis, Phys. Rev. B **63**, 144524 (2001).
[38] M. C. Gordillo and J. Boronat, Phys. Rev. B **85**, 195457 (2012).
[39] L. Vranjes Markic, P. Stipanovic, I. Beslic, and R. E. Zillich, Phys. Rev. B **88**, 125416 (2013).